CAPACITIVE VIBRATION-TO-ELECTRICITY ENERGY CONVERTER WITH INTEGRATED MECHANICAL SWITCHES

Yi Chiu, Victor F.G. Tseng
Department of Electrical and Control Engineering, National Chiao Tung University
1001 Ta Hsueh Road, Hsinchu, 300, Taiwan, R.O.C.
Tel: +886-3-573-1838, Fax: +886-3-571-5998

Abstract

This paper presents the design of a MEMS capacitive vibration-to-electricity energy converter with integrated mechanical switches for precise timing control. Integrated lateral mechanical contact switches have the advantage of zero leakage current, low energy consumption and synchronous operation. The new design can provide an output power of 31μW at a 40V output voltage from the targeted vibration with an acceleration of 2.25 m/s^2 at 120 Hz. The device is fabricated in SOI wafers. Device fabrication and measurements are presented.

Key Words: energy harvesting, vibration, mechanical switches, variable capacitor, SOI wafers

1. INTRODUCTION

Low power CMOS VLSI technology has enabled the development of such applications as wireless sensor networks [1] or personal health monitoring [2]. Energy scavenging from ambient natural sources, such as vibration [3], radioisotope [4] and ambient heat [5], is attracting much recent interest as a self-sustainable power source for low-power applications. This paper presents a capacitive vibration-to-electricity energy converter fabricated in a silicon-on-insulator (SOI) wafer.

In the operation of the capacitive energy converter, leakage current, power consumption, and timing control of the switches are crucial to conversion efficiency. In this paper, a novel integrated mechanical switch design is proposed. Compared to traditional design with diodes or active electric circuit components, the mechanical switches have the advantage of zero leakage current, low power consumption and synchronous operation.

2. DESIGN

The targeted vibration source in our design is 2.5 m/s^2 at 120 Hz [6]. The converter is composed of a 3.6 V auxiliary battery supply V_{in}, a vibration-driven variable capacitor C_v and an output storage capacitor C_{stor} connected with the load R_L, as shown in Fig. 1 [6]. C_v is charged by V_{in} through SW1 at its maximum C_{max}, and discharged to C_{stor} through SW2 at its minimum C_{min}. To achieve high conversion efficiency, the charge-discharge cycles must be timed precisely with the variation of the capacitance. Since the operation of the converter depends on the mechanical oscillation of a proof mass, mechanical switches that turn on or off according to the position of the proof mass can work synchronously in the converter.

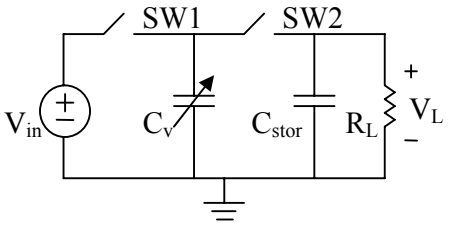

Fig. 1: Operation of the electrostatic energy converter

2.1 Static analysis

2.1.1 Variable capacitor

The variable capacitor C_v is formed by an in-plane gap-closing comb structure [7], as shown in Fig. 2(a). Silicon nitride (ε_r=7) is deposited on finger sidewalls to prevent finger shortage and increase C_{max} (without increasing C_{min}). The comb fingers are designed with "bumps" on the sidewalls to maintain the minimum air gap even in the presence of etching tolerance, as shown in Fig. 2(b).

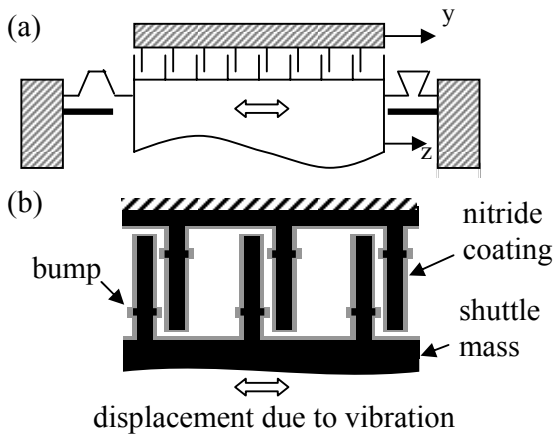

Fig. 2: (a) In-plane gap-closing variable capacitor, (b) bumps on comb fingers

With a minimum air gap of 0.5 μm, sidewall silicon nitride thickness of 500 Å, device thickness of 200 μm, device area of 1 cm^2, and V_{in} of 3.6V, Fig. 3 shows the output power, as a function of the initial finger gap distance. It also shows the maximum electrostatic spring constant caused by the constant charge Q on the variable capacitor C_v. The effect of the electrostatic spring constant will be discussed in the dynamic analysis. Therefore, an output power of 31 μW can be obtained with an initial finger gap of 26 μm in our device.

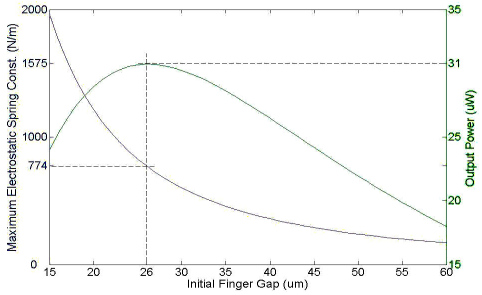

Fig. 3 Output power and maximum b_e vs. initial finger gap

2.1.2 SW1 design

SW1 should ideally be closed when the movable electrode of the variable capacitor is near the maximum displacement, and opened immediately after charging is finished. In our design, one end of SW1 is attached to the movable electrode of C_v and the other attached to the charging terminal, as shown in Fig. 4. SW1 laterally contacts at the maximum displacement (C_{max}) position. With the extra displacement the finger geometry can allow, SW1 is designed with a spring structure to provide a 1.16-mN restoring force at an extra displacement of 1 μm for low contact resistance during charging.

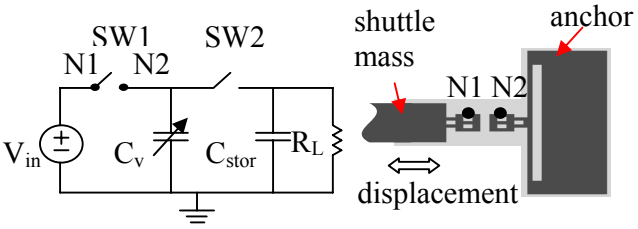

Fig.4 SW1 as a contact mechanical switch

2.1.3 SW2 Design

SW2 closes when the movable electrode of the variable capacitor moves to the center position. At this position, the terminal voltage of C_v has a maximum value V_{max}. This high voltage is used to induce electrostatic pull-in between nodes A and B, as shown in Fig. 5. When pull-in occurs, the movable node A is attracted by the electrostatic force to node B but contacts with node C before touching node B. The spring connected to node A and the gap between nodes A and B are designed such that the pull-in voltage is smaller but close to V_{max}.

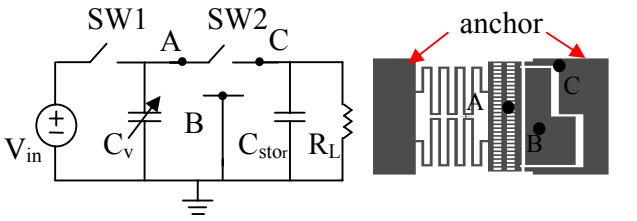

Fig. 5: SW2 as a pull-in contact switch

2.2 Dynamic analysis

The dynamic analysis is used to decide the mechanical spring constant k and proof mass m in order to ensure adequate resonance displacement in the presence of the targeted vibration. The equation of motion is

$$m\ddot{z}+b_e z+b_m(z,\dot{z})\dot{z}+kz=-m\ddot{y} \qquad (1)$$

where y is the displacement of the device frame caused by vibration, z is the displacement of the shuttle mass with respect to the device frame, $b_m(z,\dot{z})\dot{z}$ is the mechanical damping force, and $b_e z$ is the electrostatic force acting on the movable structure.

The electrostatic force $b_e z$ is equivalent to a spring force with a negative spring constant b_e, whose value varies with time in the charge-discharge cycles. The total spring constant of the system becomes $k'=k+b_e$. In order to maintain a steady resonance, the mechanical spring constant k should be larger than b_e to reduce its effect on the system dynamics. Therefore, the mechanical spring constant k and the electrostatic spring constant b_e, which depends on the static variable capacitor design, must be found from the iteration between the static and dynamic analyses.

The output power of the optimized design is shown in Fig. 3. The dynamic response simulated by Simulink in Fig. 6 shows a saturation output voltage of 40V and output power of 31 μW for a load of 50 MΩ.

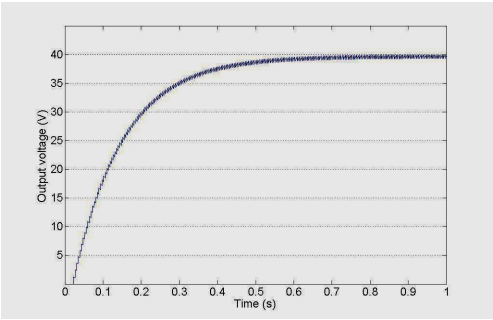

Fig.6: Dynamic response of output voltage

The effect of switch timing error on the output power is also studied by Simulink simulation. For example, SW2 should turn on when the movable electrode of the variable capacitor is at the center position (C_{min}). In this case, the energy in C_v can be transferred to C_{stor} at its maximum voltage, If not, the energy is transferred at a lower voltage and the efficiency will be reduced. Fig. 7 shows the simulated output power vs. timing error of SW2. It can be seen that a 500 μs timing error causes the output power to drop by 10%.

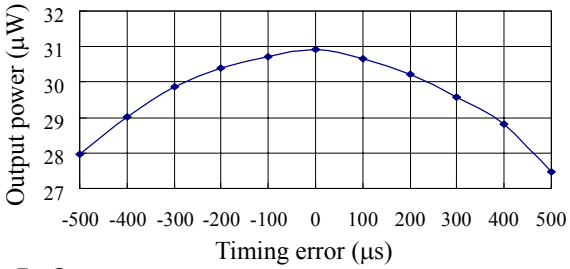

Fig.7: Output power vs. timing error

3. FABRICATION

The device was fabricated in a silicon-on-insulator (SOI) wafer with a 200-μm-think low-resistance device layer. The device structure was first defined by inductively-coupled plasma (ICP) etching. Silicon nitride was then deposited by low-pressure chemical vapor deposition. The backside handle layer under the fingers was then removed by ICP etching to reduce parasitic capacitance. The structure was released in buffered HF solution. Gold or aluminium was sputtered for metallic contact.

Fig. 8 shows the schematic cross section view of the fabricated device with the external mass attached. Fig. 9 shows the SEM micrographs of a device after the first ICP process. Devices have been successfully fabricated.

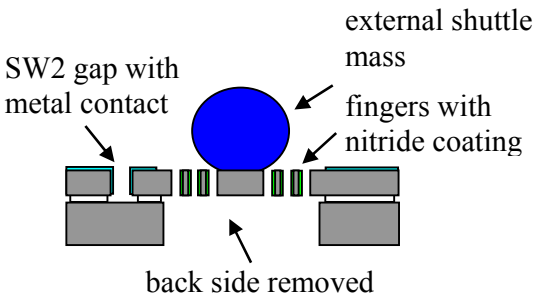

Fig. 8: Cross section view of the fabricated device

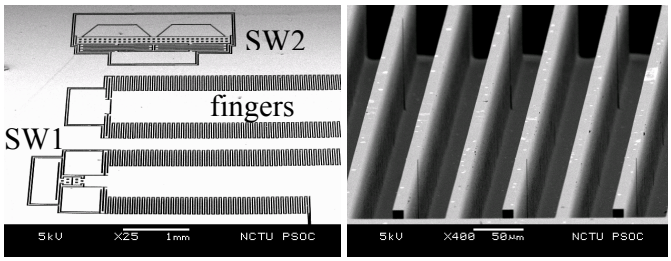

(a) (b)

Fig.9: (a) Device overview, showing comb fingers, SW1 and SW2, (b) close-up view of fingers

4. MEASUREMENT

4.1 Mechanical measurement

The relative displacement of the proof mass with a 4 gram metal ball attached was measured with a MEMS Motion Analyzer (MMA), as shown in Fig. 10. The amplitude response shows that the resonant frequency is around the expected 120 Hz. The resonance has a low quality factor about 4. The reason for this low value is currently under investigation.

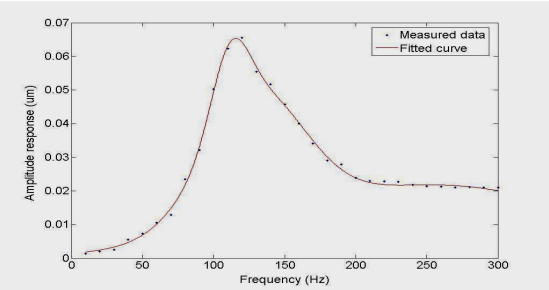

Fig.10: MMA measurement of a device with external mass

4.2 Electrical measurement

The electrical measurement was conducted using an INSTEK-LCR-816 LCR meter. The measured variable capacitance changes from 120 pF to about 300 pF. The results indicate a parasitic capacitance of about 60 pF in the device. A parallel parasitic conductance of about 800 kΩ to 1 MΩ was also observed by the LCR meter. This is probably due to partial shortage caused by the metallization at the bottom between electrodes. If a series capacitor is used to block the DC path in the device, a preliminary measurement shows a 200 nW output power before the external mass is attached. Further measurement is in progress.

5. CONCLUSION

The design and analysis of a micro vibration-to-electricity energy converter with integrated mechanical switches are presented. Contact and pull-in mechanism for mechanical switch design have the advantage of zero charge leakage and synchronous operation to the external vibration. Device fabrication was completed and detailed measurement is in progress.

REFERENCES

[1] J. M. Rabaey, et al., "Picoradio supports ad hoc ultra low-power wireless networking", *IEEE Computer,* vol. 33, pp. 42-48, 2000.

[2] R. Tashiro, et al., "Development of an electrostatic generator that harnesses the motion of a living body: use of a resonant phenomenon", *JSME International Journal Series C*, vol. 43, no. 4, pp. 916-922, 2000.

[3] S. Roundy, et al., "Micro-electrostatic vibration-to-electricity converters," in *Proc. International Mechanical Engineering Congress and Exposition*, 39309, 2002.

[4] A. Lal, et al., "Pervasive power: a radioisotope-powered piezoelectric generator," *IEEE Pervasive Computing*, vol. 4, pp. 53-61, 2005.

[5] T. Douseki, et al., "A Batteryless wireless system uses ambient heat with a reversible-power-source compatible CMOS/SOI DC-DC converter" in *Proc. IEEE International Solid-State Circuits Conference*, pp. 388-389, 2003.

[6] Y. Chiu, et al., "MEMS design and fabrication of an electrostatic vibration-to-electricity energy converter," *Microsystem Technologies*, vol. 13, no. 11-12, pp. 1663-1669, 2007.